

# Intersecting Parallel-Plate Waveguide Loaded Cavities for Dual-Mode and Dual-Band Filters

Eric J. Naglich, *Student Member, IEEE*, Juseop Lee, *Member, IEEE*, Hjalti H. Sigmarsson, *Member, IEEE*, Dimitrios Peroulis, *Member, IEEE*, and William J. Chappell, *Senior Member, IEEE*

**Abstract**—Dual-mode and/or dual-band microwave filters often employ high quality factor ( $Q$ ), physically large, and frequency static cavity resonators or low  $Q$ , compact, and tunable planar resonators. While each resonator type has advantages, choosing a dual-mode and/or dual-band resonator type is often limited by these extremes. In this paper, a new dual-mode and/or dual-band resonator is shown with  $Q$  (360–400) that is higher than that of planar resonators while being frequency tunable (6.7% tuning range) and compact relative to standard cavity resonators. In addition, both degenerate modes of the resonator are tunable using a single actuator. The resonator is used in a single-resonator two-pole filter design and a double-resonator dual-band filter design. An analytical model is developed and design techniques are given for both designs. Measured results confirm that the proposed resonator fits between the design spaces of established dual-mode and/or dual-band resonator types and could find application in systems that require a combination of relatively high  $Q$ , tuning capability, and ease of integration.

**Index Terms**—Filters, microwave filters, multi-mode filters, passive filters, tunable filters.

## I. INTRODUCTION

DUAL-MODE resonator filters are often used in applications where volume and weight are critical design parameters, including satellite and mobile systems [1]. Past dual-mode filter structures have utilized rectangular [2], [3], circular [4], triangular [5], and other shaped planar resonators [6], as well as metal cavity [7], dielectric-resonator-loaded metal cavity [8],

Manuscript received November 20, 2012; revised March 09, 2013; accepted March 12, 2013. Date of publication April 09, 2013; date of current version May 02, 2013. This work was supported by the Defense Advanced Research Projects Agency (DARPA) under the Purdue Evanescent-Mode Cavity Filter Study Program. The work of E. J. Naglich was supported by the Department of Defense (DoD) through the National Defense Science and Engineering Graduate Fellowship (NDSEG) Program. The work of J. Lee was supported by the Basic Science Research Program through the National Research Foundation of Korea (NRF) funded by the Ministry of Education, Science, and Technology (2012R1A1A1004665).

E. J. Naglich and W. J. Chappell are with the Integrated Design of Electromagnetically-Applied Systems (IDEAS) Microwave Laboratory, Purdue University, West Lafayette, IN 47907 USA (e-mail: enaglich@purdue.edu; chappell@purdue.edu).

J. Lee is with the Department of Computer and Communications Engineering, Korea University, Seoul 136-701, Korea (e-mail: ifsnow@ieee.org).

H. H. Sigmarsson is with the School of Electrical and Computer Engineering, Oklahoma University, Norman, OK 73019 USA (e-mail: h.sigmarsson@ou.edu).

D. Peroulis is with the Adaptive Radio Electronics and Sensors (ARES) Group, Department of Electrical and Computer Engineering, Purdue University, West Lafayette, IN 47907 USA (e-mail: dperouli@purdue.edu).

Color versions of one or more of the figures in this paper are available online at <http://ieeexplore.ieee.org>.

Digital Object Identifier 10.1109/TMTT.2013.2255887

and strontium–titanate resonators [9]. All of these structures offer their own respective advantages. Planar dual-mode structures can have comparatively low volume and weight compared with other dual-mode filter structures. In addition, the required surface area for a planar dual-mode filter can be further reduced using meandering [10]. In [10], 68% size reduction of a conventional square dual-mode resonator is shown through meandering. Dual-mode filters can also have frequency tuning capability through the use of varactors [11]. In [11], a 35% frequency tuning dual-mode bandpass filter is shown. However, tunable planar filters often have low resonator quality factors ( $Q$ ) on the order of 20–200 due to substrate and tuning element losses.

The volume and weight of metal cavity dual-mode filters can be significantly reduced while retaining high resonator  $Q$  values on the order of 1000–10 000 by using dielectric loading, rectangular ridge resonators [12], or transverse magnetic modes [13]. Substrate integrated waveguide (SIW) dual-mode filters [14]–[16] add simple integration of a filter with other system components at a slight cost to  $Q$  due to increased dielectric losses compared with an air-filled cavity. However, these resonators are difficult to electronically tune due to their resonator field distributions. Additionally, while these technologies provide valuable volume and weight savings over single-mode air-filled metal cavity filters, they still have dimensions that are significant fractions of a wavelength at their operating frequencies.

An additional feature of some dual-mode resonator structures is the capability to produce dual-band filter responses through the use of multiple sets of coupled resonances from the same resonator. Examples of dual-band filters that use dual-mode resonators can be seen in [1]–[4], [7], [17], and [18], with most using resonators that belong to the planar or metal cavity categories described above. Planar dual-band filters where either one or both of the passbands are tunable have also been presented [19], [20]. In [19], the lower passband is tunable over a 22.2% frequency range, and the upper passband is tunable over a 19.6% frequency range. In [20], over 17% tuning of the upper passband is achieved while the lower passband remains static.

Currently, dual-mode and dual-band filter designers must choose between compact tunable low- $Q$  planar designs or potentially bulky, static, high- $Q$  cavity, or dielectric resonator designs. In some applications it would be useful to have a resonator structure that has some of the compactness and tuning capability of past planar designs while retaining a  $Q$  approaching those of cavity-based designs. This paper presents a new type of highly loaded coaxial cavity resonator filter that can fill this need. In contrast to previous highly loaded coaxial cavity resonator filters with wide spurious-free ranges [21]–[23], the proposed resonator has a loading post, the center

conductor of the coaxial structure, which is split into multiple pieces to create new modes that can be used to create filter responses. While the new resonator structure can be made using any type of conductor-walled cavity such as machined bulk metal, the measured implementations shown in this paper use plated via-defined substrate-integrated cavities [21]–[26]. However, substrate-integrated cavities are not required to use the resonator presented in this paper. A dual-mode two-pole filter using one of these resonators is shown in which the fundamental mode and both degenerate resonances can be tuned with a single actuator. This is a significant operational advantage over both past dual-mode filter designs and past single-mode highly loaded coaxial cavity resonator filters [21] because it simplifies potential control circuits. Finally, a tunable dual-band filter with a two-pole response in its lower band and a four-pole response in its higher band is shown that uses two of the new highly loaded coaxial cavity resonators. This structure is unique compared with previous dual-band filter implementations that use two resonances per physical resonator because the first band is created using the fundamental mode of the resonators and the second band is created using both of the next higher degenerate modes of the resonators for a total of three resonances per physical resonator.

## II. INTERSECTING PARALLEL-PLATE WAVEGUIDE LOADED RESONATORS

Previously presented tunable coaxial cavity filters are tuned by physically modulating a small gap between the capacitive loading post and the wall of the cavity. In order to enable dual-band and dual-mode responses, the loading post of a coaxial cavity resonator is sliced into several wedge-shaped pieces in this work, creating degenerate modes in the resulting intersecting parallel-plate waveguide sections inside the post. A model of a highly loaded coaxial cavity where the loading post has been sliced into four wedges can be seen on the left side of Fig. 1. The four wedge pieces create two orthogonal parallel-plate waveguide sections inside the loading post. Fig. 1 shows important design parameters of the intersecting parallel-plate waveguide loaded resonator, including the cavity radius ( $b$ ), loading post radius ( $a$ ), cavity height ( $h$ ), span of the gaps between wedge pieces ( $x$ ), and gap between the four-wedge loading post and the top wall of the cavity ( $g$ ). These design parameters can be used to manipulate the typical fundamental mode of the highly loaded coaxial cavity resonator as well as three new additional modes that are created through the division of the loading post into four wedge pieces. The right side of Fig. 1 shows ANSYS HFSS simulated vector plots of the electric field (*left*) and magnetic field (*right*) of: fundamental (a); degenerate (b and c); and first higher-order spurious modes (d) of the resonator. The degenerate modes are orthogonal in space but share the same underlying geometry and boundary conditions. Therefore, in the absence of perturbation the degenerate modes occur at the same frequency.

An analytical model for fast approximation and theoretical understanding of the four modes shown in Fig. 1 can be constructed through expansion of the electromagnetic analysis in [27]. The fundamental mode [see Fig. 1(a)] frequency is modeled by approximating the cavity inductance as the inductance

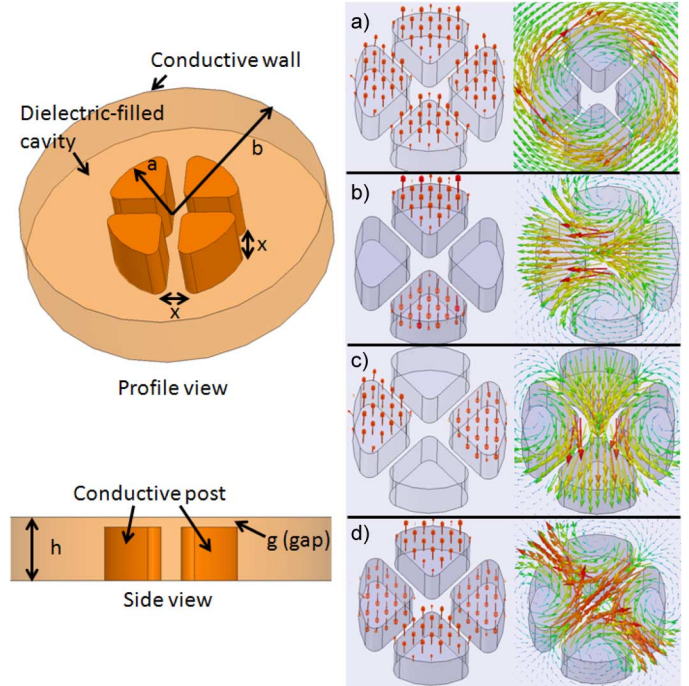


Fig. 1. Profile and side views of a four-wedge intersecting parallel-plate waveguide loaded coaxial cavity resonator.  $E$  (*left*) and  $H$  (*right*) fields of: a) fundamental mode, b) and c) degenerate modes, and d) first spurious mode.

of a length  $h - g$  of coaxial cable and the cavity capacitance as the parallel-plate capacitance between the loading post wedges and the top wall of the cavity and the capacitance of a length  $h - g$  of coaxial cable in parallel. The fundamental mode frequency in terms of the resonator geometry is

$$f_f = \frac{1}{2\pi} \sqrt{\frac{1}{LC}} = \frac{1}{2\pi} \sqrt{\frac{2\pi}{\mu(h-g) \ln\left(\frac{b}{a_{\text{eff}}}\right) (C_{\text{pp}} + C_{\text{coax}})}} \quad (1)$$

where  $C_{\text{pp}}$  is the parallel-plate capacitance between the loading post top and cavity wall incorporating the fringing field approximation in [28] and given by

$$C_{\text{pp}} = \frac{\epsilon}{g} \left( \pi a_{\text{eff}}^2 + g a_{\text{eff}} \ln\left(\frac{16\pi a_{\text{eff}}}{g} - 1\right) \right) \quad (2)$$

and  $C_{\text{coax}}$  is the capacitance of a length  $h - g$  of coaxial cable given by

$$C_{\text{coax}} = \frac{2\pi\epsilon(h-g)}{\ln\left(\frac{b}{a_{\text{eff}}}\right)}. \quad (3)$$

Note that these formulas account for the reduction in the parallel-plate capacitor area caused by  $x$  by using an effective post radius  $a_{\text{eff}}$  given by

$$a_{\text{eff}} = \sqrt{a^2 - \frac{4ax}{\pi} + \frac{x^2}{\pi}}. \quad (4)$$

The same parallel-plate capacitor model can be used to determine an expression for the energy stored in the electric field for the degenerate modes. However, the capacitance of the intersecting parallel-plate waveguide sections inside the loading

post, which is in parallel with the parallel-plate capacitance between the post and cavity wall, must also be taken into account to accurately model the degenerate modes. The energy stored in the electric field of the degenerate modes can be written as

$$W_e = \frac{\epsilon}{4} \iiint_V |\bar{E}|^2 dV = \frac{\epsilon}{2} g A_{\text{eff}} E_0^2 \quad (5)$$

where  $E$  is the electric field,  $\epsilon$  is the permittivity of the dielectric inside the cavity,  $A_{\text{eff}}$  is the effective area of the capacitance for the degenerate mode, and  $E_0$  is the magnitude of the electric field. For the degenerate modes, the magnetic field concentration is much higher in the volume between the post wedges than in the volume exterior to the loading post if  $x$  is small relative to  $a$ , so it is also assumed that all of the current for this mode is flowing on the parallel-plate walls interior to the loading post. The magnetic field in the resonator can be calculated from the current density on the parallel-plate walls interior to the loading post. Therefore, the energy stored in the magnetic field of the degenerate modes can be written as

$$W_m = \frac{\mu}{4} \iiint_V |\bar{H}|^2 dV = \frac{\mu(h-g)x\epsilon^2 E_0^2 \omega^2 A_{\text{eff}}^2}{8a} \quad (6)$$

where  $\mu$  is the permeability of the dielectric inside the cavity,  $x$  is the gap between wedge pieces, and  $\omega$  is radian frequency. Equating (5) and (6) at resonance yields the degenerate mode frequency,  $f_d$ , in terms of the resonator geometry

$$f_d = \frac{1}{2\pi} \sqrt{\frac{4a}{\mu(h-g)x \left( \frac{C_{\text{pp}}}{2} + C_{\text{ppw}} \right)}} \quad (7)$$

where  $C_{\text{ppw}}$  is the capacitance of one of the intersecting parallel-plate waveguide sections inside the loading post and is defined as

$$C_{\text{ppw}} = \epsilon(2a-x) \left( \frac{(h-g)}{x} + \frac{1}{\pi} + \frac{1}{\pi} \ln \left( \frac{2\pi(h-g)}{x} \right) \right). \quad (8)$$

Note that the dimension  $h-g$  is the width of the parallel-plate waveguide section, and the dimension  $x$  is its height. A fringing field approximation from [29] is also used in (8). An expression for the first higher order spurious mode frequency can be obtained from (7) by reducing the effective area of the parallel-plate capacitance by a factor of 2. Therefore, the first higher order spurious mode frequency is

$$f_s = \frac{1}{2\pi} \sqrt{\frac{4a}{\mu(h-g)x \left( \frac{C_{\text{pp}}}{4} + C_{\text{ppw}} \right)}}. \quad (9)$$

Note that  $C_{\text{ppw}}$  is modeled to be the same for both  $f_d$  and  $f_s$  because the magnetic field curls around a single loading post wedge piece in the analysis of  $f_s$ . Although it encounters a bend along this path, it encounters the same length of parallel-plate waveguide interior to the loading post as in the analysis of  $f_d$  where the magnetic field traverses the diameter of the loading post. The effect of the bend is only significant for large ratios of

Table I  
DESIGN PARAMETERS OF SIMULATED DUAL-MODE CAVITIES

Cavity	$a$ (mm)	$b$ (mm)	$x$ (mm)	$h$ (mm)	$x/a$ (%)
1	2.0	8.0	0.4	3.0	20
2	3.0	8.0	0.9	3.0	30
3	4.0	8.0	1.6	3.0	40
4	5.0	8.0	2.5	3.0	50

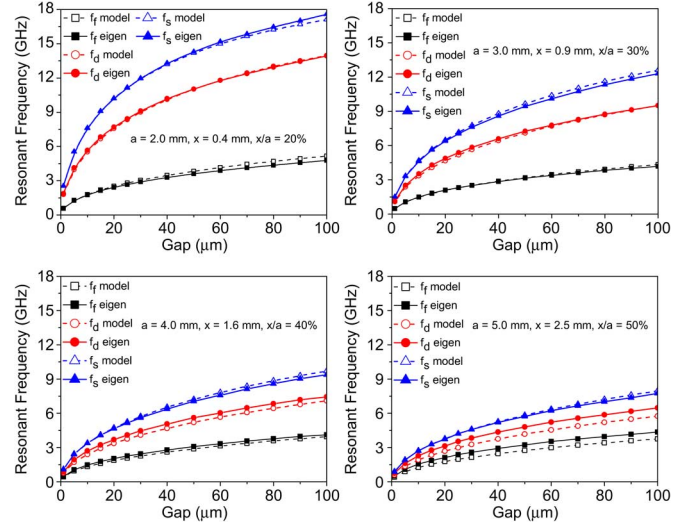


Fig. 2. Resonant frequencies calculated by the analytical model and ANSYS HFSS eigenmode simulation of the cavities described in Table I.

$x$  and  $a$  that are beyond the scope of the design space focused on in this paper.

In order to determine the accuracy of the model described above, it was checked against HFSS eigenmode simulations of dual-mode highly loaded coaxial cavities with the dimensions shown in Table I. For all cases, the permittivity and permeability were set to their respective free-space values and  $b$  and  $h$  were kept constant to highlight the effects of varying values and ratios of  $a$  and  $x$ . Fig. 2 shows a comparison of the calculated resonant frequency versus gap ( $g$ ) from the analytical model and ANSYS HFSS eigenmode simulations for the four modes discussed above. Note that as the ratio of  $a$  and  $x$  changes, the ratio of the frequencies of the fundamental and degenerate modes changes. Using this ratio, the frequency spacing of the fundamental and degenerate modes can be set for dual-band filter design.

It can be seen that the resonant frequencies calculated by the analytical model are very close to those calculated by the eigenmode simulations for small gaps ( $g$ ) and small  $x$ . The analytical model becomes less accurate for large  $g$  because the fringing field capacitance approximation used in (2) is not exact. Similarly, it becomes less accurate for large  $x$  because the effect of the fringing field approximation is magnified in this situation. While the analytical model has limitations at the extremes of the design space, it is accurate enough to be used to obtain a starting point for full-wave simulation and simple enough to provide understanding of the resonator's operation.

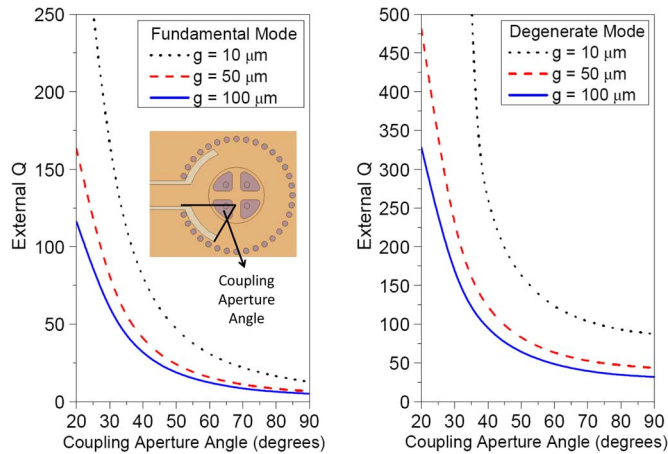


Fig. 3. External  $Q$  versus coupling aperture sweep angle for the fundamental and degenerate modes of the proposed resonator.

### III. BANDPASS FILTER DESIGN USING PARALLEL-PLATE WAVEGUIDE LOADED CAVITIES

In order to design a filter with a specific type of resonator, external coupling and inter-resonator coupling values available from that resonator with particular coupling structures must be known and understood. This section will show design graphs of the simulated available coupling values of a parallel-plate waveguide loaded coaxial cavity with specific coupling structures. These structures are meant to serve as examples and are not exclusive. Values for external coupling from a port to a resonator, intra-resonator coupling between two degenerate modes within a single cavity, and inter-resonator coupling between two cavities will be shown.

#### A. External Coupling

Many highly loaded coaxial cavity resonators and filters use apertures to achieve external coupling, and aperture coupling can be used in parallel-plate waveguide loaded coaxial cavities as well. A simulation model of a resonator with aperture coupling can be seen in the inset in Fig. 3. The aperture is created by sweeping the end of the insulated traces of a coplanar waveguide transmission line along an angle. The simulation model consists of an 8-mm radius substrate-integrated cavity defined by plated vias and a copper loading post of radius 3.55-mm cut into four wedges. Note that the geometry of this resonator is the same as that used in the fabricated example shown later in this paper, and a more detailed description will be given in Section IV. Additionally, while the analysis above assumed solid cavity walls and bulk metal loading post elements, the performance of highly loaded via-defined geometries can still be well predicted by the analysis because the capacitance between the top of the loading post and the top wall of the resonator dominates the total capacitance. For less-loaded structures, bulk metal is recommended. For this study, the aperture sweep angle, defined graphically in Fig. 3, was swept from  $20^\circ$  to  $90^\circ$ . External coupling values were extracted according the method described in [30] for the fundamental and degenerate modes for gaps ( $g$ ) of 10, 50, and  $100 \mu\text{m}$ . Fig. 3 shows that the aperture sweep angle and gap ( $g$ ) parameters can be used to obtain desired external coupling values. The ratio of the fundamental mode and degenerate mode

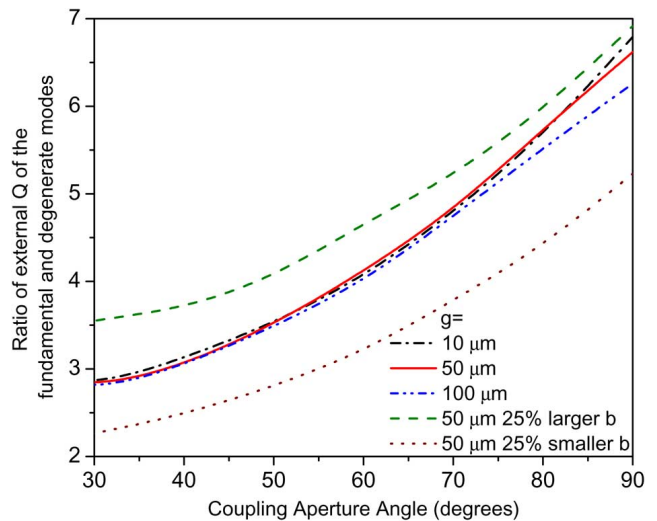


Fig. 4. Ratio of external  $Q$  of the fundamental and degenerate modes versus coupling aperture sweep angle for resonators with various outer radii ( $b$ ).

external coupling values can be seen in Fig. 4 for different sizes of cavities. Three lines in Fig. 4 show ratios of the external coupling values shown in Fig. 3 for three values of  $g$ . The other two lines show ratios of the external coupling values of resonators with 25% larger or smaller outer diameters ( $b$ ), respectively, with a  $g$  of  $50 \mu\text{m}$ . Fig. 4 shows that the outer diameter ( $b$ ) of the cavities can be designed to provide different ratios of external coupling, enabling the design of dual-band filters with independent bandwidths. Such a change effectively changes the relative amount of capacitive loading in the cavity, or equivalently, the resonator's characteristic impedance at different frequencies. In summary, a filter designer can set the ratio of external coupling values using the technique shown in Fig. 4 and then set the absolute coupling values by using the coupling aperture sweep angle, as shown in Fig. 3.

#### B. Intra-Resonator Coupling

Intra-resonator coupling refers to the coupling between degenerate modes inside a single cavity. It can be implemented with an additive or subtractive feature in one corner of the cavity's loading post. Alternatively, it can be implemented with a via or other conductive element that is located radially outward from the loading post. A mode splitting feature can be seen in the inset of Fig. 5 on the upper right corner of the loading post. Fig. 5 also shows  $k_{\text{intra}}$  values for mode splitting feature radii from 0.1 to 1 mm using a similar cavity as was used for the external coupling simulations above.  $k_{\text{intra}}$  is defined as

$$k_{\text{intra}} = \frac{f_b^2 - f_a^2}{f_b^2 + f_a^2} \quad (10)$$

where  $f_b$  and  $f_a$  are the frequencies of the peaks seen in the transmission response when a pair of coupled resonances is coupled to the measurement ports using weak external coupling. Fig. 5 shows that relatively small perturbations to the loading post can produce a wide range of values of  $k_{\text{intra}}$  while not strongly affecting the fundamental mode frequency. Note also that  $k_{\text{intra}}$  is not a strong function of the gap ( $g$ ) between the

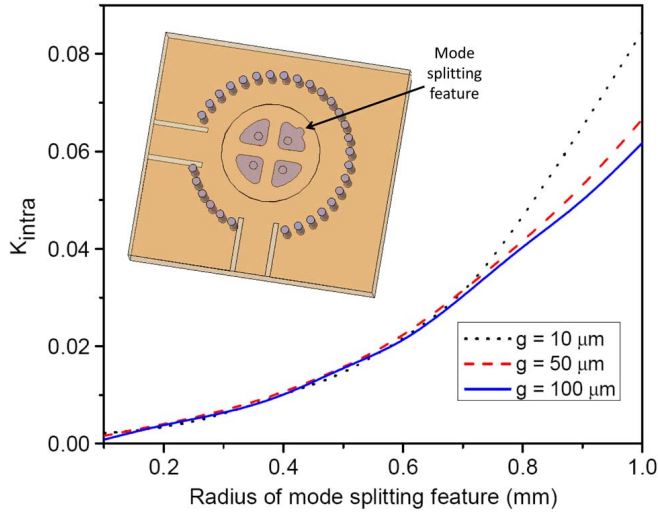


Fig. 5. Intra-resonator coupling,  $k_{\text{intra}}$ , versus radius of mode-splitting post feature.

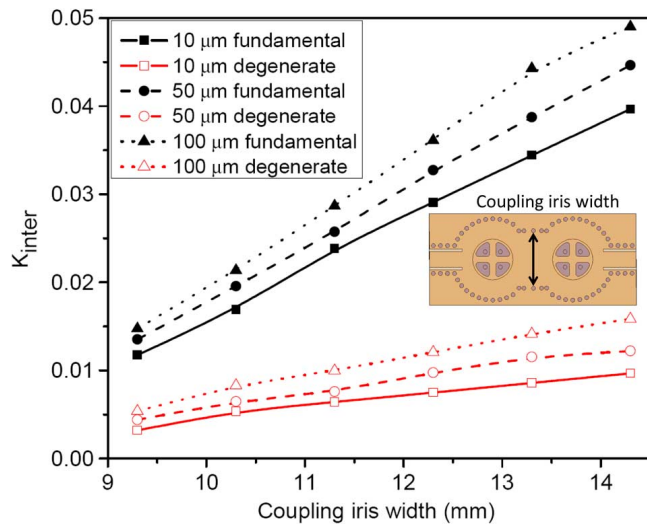


Fig. 6. Inter-resonator coupling,  $k_{\text{inter}}$ , versus coupling iris width.

loading post and top wall of the cavity, allowing  $g$  to be used as a design parameter for external coupling.

### C. Inter-Resonator Coupling

Inter-resonator coupling between cavity resonators can be implemented with waveguide irises. An example of a waveguide iris used to couple two parallel-plate waveguide loaded substrate-integrated cavities can be seen in the inset in Fig. 6. Fig. 6 also shows that inter-resonator coupling,  $k_{\text{inter}}$ , is a function of coupling iris width and  $g$ .  $k_{\text{inter}}$  is defined as

$$k_{\text{inter}} = \frac{f_b^2 - f_a^2}{f_b^2 + f_a^2} \quad (11)$$

where  $f_b$  and  $f_a$  are the frequencies of the peaks seen in the transmission response when a pair of coupled resonances is coupled to the measurement ports using weak external coupling. Note that  $k_{\text{inter}}$  is also a function of the spacing between the coupled cavities and any perturbations in the iris, but these concepts

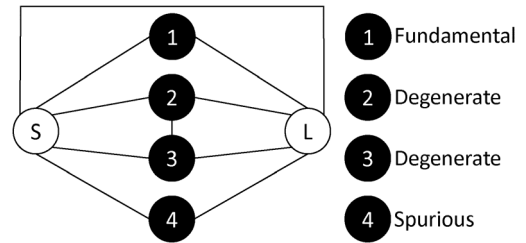


Fig. 7. Coupling-routing diagram for all four resonances of interest of the two-pole single-resonator bandpass filter.

will not be shown here. Additionally, low- or high-pass structures can be added in parallel with the iris to affect the frequency dependence of the coupling iris [21], effectively changing the ratio of inter-resonator coupling for the fundamental and degenerate modes of a pair of parallel-plate waveguide loaded cavities since the fundamental and degenerate modes occur at different frequencies. Using waveguide irises,  $n$ -pole filters that use two degenerate modes per resonator can be designed, where  $n$  is an even integer. Now that the coupling values and example methods to manipulate them are understood, Section IV will present design examples.

## IV. DESIGN EXAMPLES

### A. Two-Pole Single-Resonator Bandpass Filter

This section will provide an overview of the design and layout of a 1.2% 3-dB fractional bandwidth Butterworth two-pole filter that is tunable about a frequency of 4.45 GHz and uses a single intersecting parallel-plate waveguide loaded resonator. The coupling and routing diagram of the structure can be seen in Fig. 7. A coupling matrix will be shown later in this paper to describe certain aspects of the measured responses. The design utilizes a fabrication procedure that has been used by the authors previously, and more detailed descriptions of the process can be found in [22], [31], and [32]. The resonator was designed as a substrate integrated resonator in a 3.175-mm-thick Rogers TMM3 ( $\epsilon_r = 3.27$ ,  $\tan(\delta) = 0.002$  @ 10 GHz) substrate, and its simulation model can be seen in Fig. 8 along with simulation results of a weakly coupled forward transmission coefficient that shows the modes used for filtering. However, it is important to note that these resonators can be implemented using a multitude of fabrication techniques ranging from standard bulk metal machining to more complicated microfabrication techniques. The geometry shown in Fig. 8 was estimated using the design equations presented in Section II and optimized using ANSYS HFSS software. In addition to what is shown in Fig. 8, the nominal gap ( $g$ ) between the loading post and the top flexible wall of the cavity was designed to be 80  $\mu\text{m}$ , and it was physically implemented by stacking three layers of 1-mil Dupont Pyralux LFO100 adhesive when laminating the flexible copper top wall of the cavity. Mechanically modulating  $g$  produces frequency tuning of the filter, and this modulation was done using 0.38-mm-thick 12.7-mm-diameter piezoelectric disk actuators from Piezo Systems Inc.

Another design aspect to note from Fig. 8 is that a plated via was used to obtain intra-resonator coupling instead of the

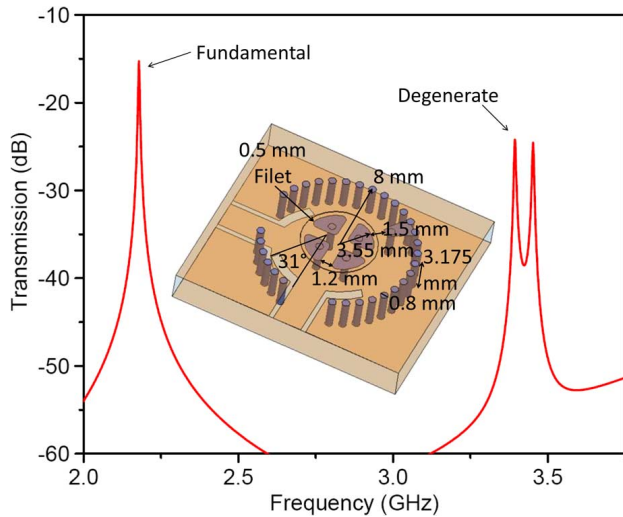
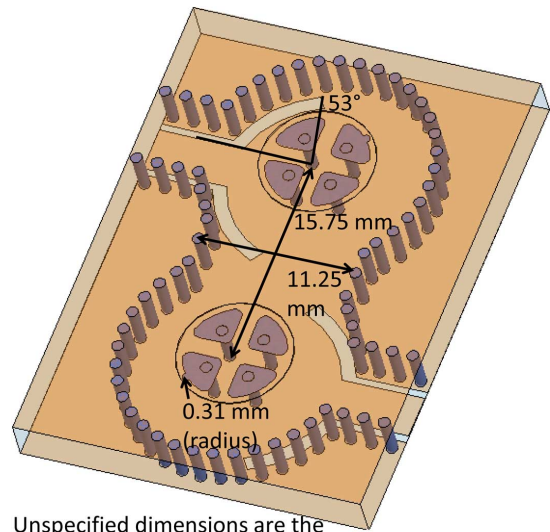


Fig. 8. Simulation model of the single-resonator dual-mode filter and simulated weakly coupled forward transmission coefficient showing fundamental and degenerate modes used for filtering. Nominal  $g = 80 \mu\text{m}$ .

mode-splitting feature on the loading post that was described in Section III, which may be more or less favorable depending on the fabrication technologies available to the designer and the required value of intra-resonator coupling. For example, a small value of intra-resonator coupling would require a small and accurately sized feature to be added to the loading post that could be outside the fabrication tolerances of some manufacturing techniques. However, a relatively large plated via could be used to implement the same amount of intra-resonator coupling if it is placed far enough away from the loading post. The position of this via was determined through optimization in simulation using the method described in [33], and it has a similar relationship to  $k_{\text{intra}}$  as the feature shown in Section III. The external coupling structures are on separate conductor layers to aid in source-to-load out-of-band isolation, and their width is 1 mm. As shown in Fig. 8, the aperture sweep angle was determined to be  $31^\circ$  by the method presented in [30]. Simulated and measured results of the two-pole filter will be shown in Section V.

### B. Double-Resonator Dual-Band Bandpass Filter

This section will describe the design of a dual-band bandpass filter with a two-pole 5.5% 3-dB fractional bandwidth Butterworth filter at 2.5 GHz and a four-pole 2% 3-dB fractional bandwidth Butterworth filter at 4.1 GHz using the fundamental and degenerate modes of two intersecting parallel-plate waveguide loaded resonators. The resonators are similar to the one described in Section IV-A, with coupling values and intra-resonator coupling structure physical implementation being the only changes. A simulation model of the structure with relevant geometrical properties labeled is shown in Fig. 9. Coupling structure geometries were determined using ANSYS HFSS simulation and the methods in [30] and [33]. In contrast to the single resonator design described in Section IV-A, an additive loading post feature was added to implement intra-resonator coupling instead of a plated via. One other interesting aspect of the design is that the resonators are physically rotated by  $180^\circ$  with respect to each other, as was originally shown in [34].



Unspecified dimensions are the same as those shown in Fig. 8.

Fig. 9. Simulation model of the double-resonator dual-band filter. Nominal  $g = 80 \mu\text{m}$ .

Designing the filter in this way has two desirable consequences. First, if coupling apertures are used to implement external coupling as they are in this design, the apertures will be further away from each other in space with this configuration. This reduces source-to-load coupling and provides more attenuation far away from the passbands of the filter. The second advantage to rotating the resonators  $180^\circ$  with respect to each other is that the fundamental and degenerate modes in both cavities constructively couple, while the next spurious mode cancels. This is a significant functional advantage that will be shown in the measured results in Section V.

Photographs showing both sides of both the two-pole single-resonator bandpass filter and the double-resonator dual-band bandpass filter can be seen in Fig. 10. The circular piezoelectric actuators can be seen in the top row of photographs with bias lines removed for clarity. The actuators are attached to the cavity resonators using silver epoxy. The plated vias that provide connection between the loading posts and the cavity walls, as well as the mode-splitting via used in the two-pole single-resonator filter, can be seen in the bottom row of the photographs.

## V. SIMULATED AND MEASURED RESULTS

The responses of the fabricated filters were measured using an Agilent Technologies N5230C PNA. Bias voltages were applied to the piezoelectric actuators using Keithley 2400 sourcemeters. Measured versus synthesized and full-wave simulation results of the single-resonator two-pole filter can be seen in Fig. 11. The measured fundamental mode is at 2.78 GHz and has 0.73-dB insertion loss. The fundamental mode can be filtered with a high-pass filter if the two-pole dual-mode response is all that is desired. Alternatively, a low-pass filter with a cutoff frequency between the fundamental and degenerate modes could be added between the ports of the filter that would act as a shunt (bandstop) feed for the fundamental mode and a series (bandpass) feed for the degenerate modes. However, the fundamental mode is shown here to demonstrate

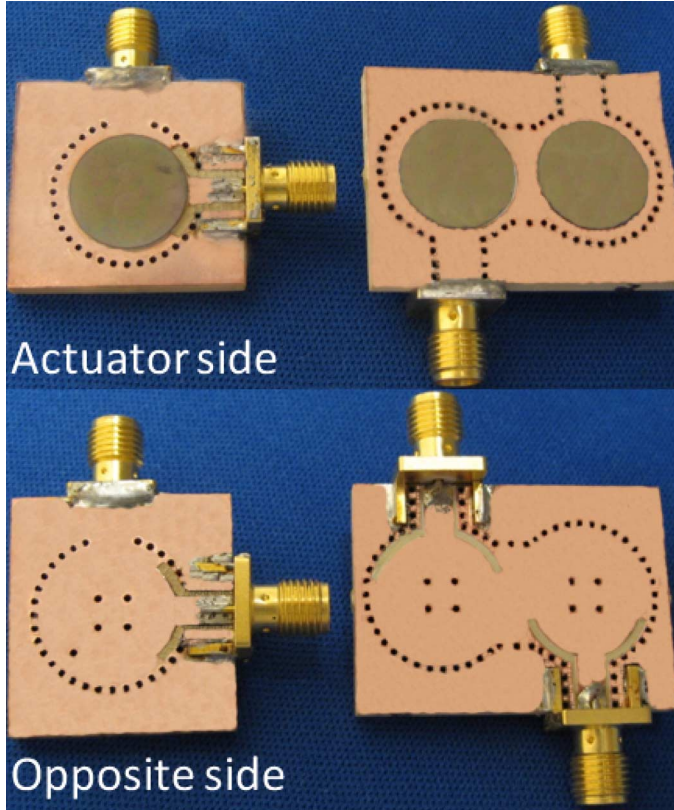


Fig. 10. Photograph showing both sides of both the two-pole single-resonator bandpass filter and the double-resonator dual-band bandpass filter.

the behavior of the new resonator structure. The measured two-pole dual-mode response is at 4.45 GHz. It has 2.80-dB insertion loss and a 3-dB bandwidth of 52 MHz, corresponding to a fractional bandwidth of 1.2% (extracted  $Q = 360$ ). The measured first spurious mode is at 5.08 GHz and has 18.75-dB insertion loss. This mode is undesired for this filter design, but it will be shown that it can be cancelled in higher order filter structures that use the proposed resonator. While the responses in Fig. 11 match well, the largest difference is the location of the transmission zero on the lower frequency side of the dual-mode two-pole filter response. This transmission zero is due to interaction of the apertures that provide external coupling and each aperture slightly coupling to the adjacent degenerate mode. These effects can be modeled in an  $N + 2 \times N + 2$  coupling matrix that corresponds to the coupling and routing diagram in Fig. 7,

$$\begin{bmatrix} 0 & 0.675 & 0.386 & -0.052 & 0.064 & 0.019 \\ 0.675 & 0 & 0 & 0 & 0 & 0.675 \\ 0.386 & 0 & -22.07 & 0.199 & 0 & -0.052 \\ -0.052 & 0 & 0.199 & -22.07 & 0 & 0.386 \\ 0.064 & 0 & 0 & 0 & -29.05 & 0.064 \\ 0.019 & 0.675 & -0.052 & 0.386 & 0.064 & 0 \end{bmatrix} \quad (12)$$

where  $-j0.082$  was added to  $M_{11}$  and  $M_{44}$  to model the bandwidth and quality factor for the fundamental and spurious modes and  $-j0.065$  was added to  $M_{22}$  and  $M_{33}$  to model the bandwidth and quality factor for the degenerate modes. The matrix in (12) was scaled to a center frequency of 2.783 GHz and a

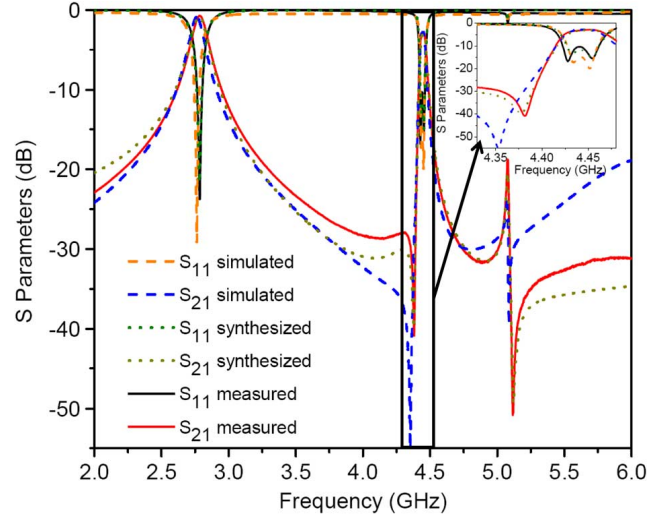


Fig. 11. Full-wave simulated versus synthesized [with (12)] versus measured results of the single-resonator dual-mode filter. Inset shows a magnified view of the dual-mode passband.

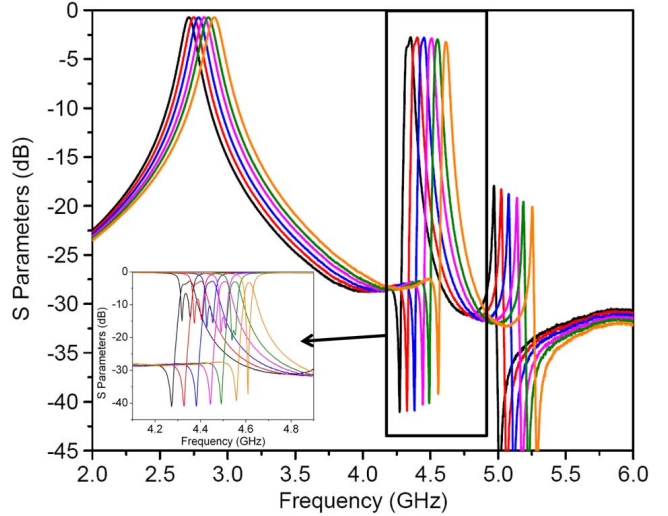


Fig. 12. Measured results of the single-resonator two-pole filter tuning over a frequency range of 4.35 to 4.65 GHz. Inset shows a magnified view of the tuning performance of the dual-mode two-pole response.

bandwidth of 122.3 MHz to correspond to the measured fundamental mode parameters. Although the coupling matrix incorporates the narrowband approximation, it still serves as a useful design tool here and describes the measured results well. Fig. 11 shows agreement between the synthesized and measured data. The discrepancy in transmission zero location in the simulated response could be attributed to slight manufacturing inaccuracies, differences between the simulation and benchtop environments, and features that were not simulated such as solder since the coupling terms that most govern its location,  $M_{SL}$ ,  $M_{S3}$ , and  $M_{2L}$ , are relatively small.

Fig. 12 shows measured results of the single-resonator two-pole filter tuning over a frequency range of 4.35 to 4.65 GHz. All four modes of interest are controlled by the same actuator, but their tuning ranges are slightly different because the tunable capacitance created by  $g$  is a different percentage of the total capacitance associated with each mode. The shown 6.7% tuning

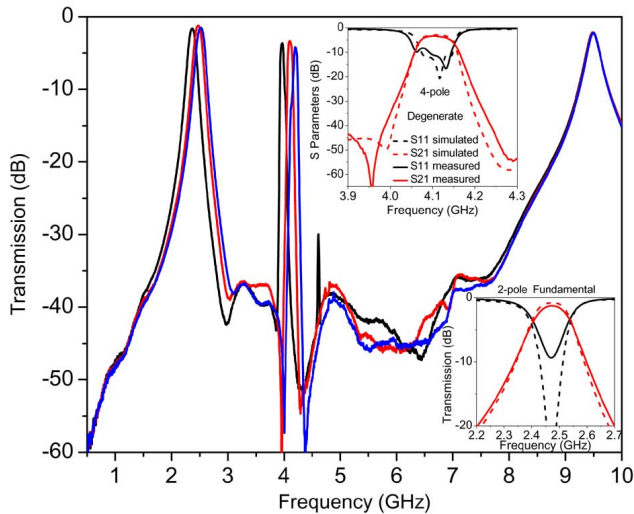


Fig. 13. Measured and simulated results of the dual-resonator dual-band filter with a two-pole response tunable about 2.5 GHz and a four-pole response tunable about 4.1 GHz. Measured results are shown with solid lines, and simulated results are shown with dashed lines.

range of the degenerate modes is much less than the octave or more tuning range that is common with highly loaded coaxial cavity filters. The cause is that a larger gap ( $g$ ) was used between the loading post and top wall of the cavity in this design (80  $\mu\text{m}$ ) in order to achieve the coupling coefficients for the desired filter bandwidth, making the center frequency less sensitive to small changes in  $g$ . Increasing this gap trades tuning range with a certain amount of actuator displacement for higher resonator impedance, higher power handling [35], and higher quality factor [23]. In a design with a larger  $g$ , an actuator with a larger range of physical motion could be used to achieve a wider tuning range. It is also worth noting that if all four modes are to be tuned together with a single actuator, the flexible copper membrane above the loading post must be relatively flat for a given  $g$  or the degenerate modes will tune at different rates. A larger  $g$  helps to mitigate this requirement.

Fig. 13 shows measured and simulated results for the double-resonator dual-band filter with a two-pole response that is tunable about 2.5 GHz and a four-pole filter that is tunable about 4.1 GHz. The two-pole response has an insertion loss of 1.26 dB and a 3-dB fractional bandwidth of 5.9%, and the four-pole response has an insertion loss of 3.34 dB and a 3-dB fractional bandwidth of 2.1% (extracted  $Q = 400$ ). Both measured responses are slightly overcoupled compared to their simulated results as can be seen in the return-loss response plotted in the insets of Fig. 13, but they still prove the concept of using multiple parallel-plate waveguide loaded coaxial cavity resonators to design higher order filter responses. As described above, the first spurious mode cancels when the resonators are oriented as they are in Fig. 9, and the first spurious mode cannot be seen in two of the three responses shown in Fig. 13. However, the spurious mode starts to appear as the resonances are tuned to slightly offset frequencies, as can be seen in the lowest frequency response in Fig. 13.

Fig. 13 shows measurement data up to 10 GHz in order to show the second spurious mode of the structure. This mode is

due to static features of the cavity and corresponds to the geometry between the loading post and the outer wall of the cavity. It was not a focus of this design, but the spurious mode can be moved higher in frequency or otherwise manipulated by removing or altering the dielectric material between the loading post and the outer wall of the cavity. While the mode looks like it is close to being critically coupled such that it could enable a triple-band response, this is a coincidence in this design. However, methods of manipulating coupling for this mode independent of the coupling for other modes used for filtering could be possible and will be the subject of future work.

## VI. CONCLUSION

A dual-mode resonator suitable for creating dual-mode and/or dual-band filter responses has been shown. The structure used a multi-section loading structure in a highly loaded coaxial cavity to create degenerate modes that do not exist in typical highly loaded coaxial cavities. An analytical model of the structure was developed that can accurately predict the frequencies of the resonances over the proposed design space relative to full-wave simulation. A single-resonator two-pole filter and a double-resonator dual-band filter were designed and fabricated using the new structure to prove the concept. The proposed dual-mode resonator combines some of the compactness and tuning capability of previous planar dual-mode/dual-band filters while maintaining a  $Q$  that approaches those of static cavity and dielectric resonator filters. Additionally, the new dual-mode resonator enables the design of dual-mode filters with resonances that tune together with a single actuator. The combination of relatively high  $Q$  and reduced tuning complexity make the proposed dual-mode resonator a unique solution for future microwave systems.

## ACKNOWLEDGMENT

The views expressed are those of the authors and do not reflect the official policy or position of the U.S. Department of Defense (DoD) or the U.S. Government. Approved for Public Release, Distribution Unlimited.

## REFERENCES

- [1] J. Lee *et al.*, "A dual-passband filter of canonical structure for satellite applications," *IEEE Microw. Wireless Compon. Lett.*, vol. 14, no. 6, pp. 271–273, Jun. 2004.
- [2] X. Y. Zhang and Q. Xue, "Novel dual-mode dual-band filters using coplanar-waveguide-fed ring resonators," *IEEE Trans. Microw. Theory Techn.*, vol. 55, no. 10, pp. 2183–2190, Oct. 2007.
- [3] T.-W. Lin *et al.*, "New dual-mode dual-band bandpass filter with quasi-elliptic function passbands and controllable bandwidths," in *IEEE MTT-S Int. Microw. Symp. Dig.*, May 23–28, 2010, pp. 576–579.
- [4] S. Luo and L. Zhu, "A novel dual-mode dual-band bandpass filter based on a single ring resonator," *IEEE Microw. Wireless Compon. Lett.*, vol. 19, no. 8, pp. 497–499, Aug. 2009.
- [5] J.-S. Hong and S. Li, "Theory and experiment of dual-mode microstrip triangular patch resonators and filters," *IEEE Trans. Microw. Theory Techn.*, vol. 52, no. 4, pp. 1237–1243, Apr. 2004.
- [6] R. Stefanini *et al.*, "Compact 2-pole and 4-pole 2.42–8 GHz dual-mode tunable filters," in *IEEE MTT-S Int. Microw. Symp. Dig.*, May 23–28, 2010, pp. 1480–1483.
- [7] S. Amari and M. Bekheit, "A new class of dual-mode dual-band waveguide filters," *IEEE Trans. Microw. Theory Techn.*, vol. 56, no. 8, pp. 1938–1944, Aug. 2008.

- [8] S. J. Fiedziuszko, "Dual-mode dielectric resonator loaded cavity filters," *IEEE Trans. Microw. Theory Techn.*, vol. MTT-30, no. 9, pp. 1311–1316, Sep. 1982.
- [9] A. Deleniv *et al.*, "Design of narrowband tunable bandpass filters based on dual mode SrTiO<sub>3</sub> disc resonators," in *IEEE MTT-S Int. Microw. Symp. Dig.*, 2002, vol. 2, pp. 1197–1200.
- [10] J.-S. Hong and M. J. Lancaster, "Microstrip bandpass filter using degenerate modes of a novel meander loop resonator," *IEEE Microw. Guided Wave Lett.*, vol. 5, no. 11, pp. 371–372, Nov. 1995.
- [11] L. Athukorala *et al.*, "Compact high linearity tunable dual-mode microstrip filters," in *Eur. Microw. Conf. Dig.*, Sep. 28–30, 2010, pp. 834–837.
- [12] S. Bastioli *et al.*, "A novel class of compact dual-mode rectangular waveguide filters using square ridge resonators," in *38th Eur. Microw. Conf.*, Oct. 27–31, 2008, pp. 626–629.
- [13] S. Bastioli *et al.*, "A new class of waveguide dual-mode filters using TM and nonresonating modes," *IEEE Trans. Microw. Theory Techn.*, vol. 58, no. 12, pp. 3909–3917, Dec. 2010.
- [14] K. Ahn and I. Yom, "A  $K_a$ -band multilayer LTCC 4-pole bandpass filter using dual-mode cavity resonators," in *IEEE MTT-S Int. Microw. Symp. Dig.*, Jun. 15–20, 2008, pp. 1235–1238.
- [15] W. Shen *et al.*, "A novel single-cavity dual mode substrate integrated waveguide filter with non-resonating node," *IEEE Microw. Wireless Compon. Lett.*, vol. 19, no. 6, pp. 368–370, Jun. 2009.
- [16] D. Deslandes and K. Wu, "Substrate integrated waveguide dual-mode filters for broadband wireless systems," in *Proc. Radio Wireless Conf.*, Aug. 10–13, 2003, pp. 385–388.
- [17] U. Rosenberg, "Multiplexing and double band filtering with common multimode cavities," *IEEE Trans. Microw. Theory Techn.*, vol. 38, no. 12, pp. 1862–1871, Dec. 1990.
- [18] J.-T. Kuo *et al.*, "Design of microstrip bandpass filters with a dualpass-band response," *IEEE Trans. Microw. Theory Techn.*, vol. 53, no. 4, pp. 1331–1337, Apr. 2005.
- [19] E. E. Djoumessi *et al.*, "Varactor-tuned quarter-wavelength dualbandpass filter," *IET Microw., Antennas, Propag.*, vol. 3, no. 1, pp. 117–124, Feb. 2009.
- [20] D. Girbau *et al.*, "Tunable dual-band filters based on capacitive-loaded stepped-impedance resonators," in *Eur. Microw. Conf. Dig.*, Sep. 29–Oct. 1, 2009, pp. 113–116.
- [21] H. Joshi *et al.*, "High-Q fully reconfigurable tunable bandpass filters," *IEEE Trans. Microw. Theory Techn.*, vol. 57, no. 12, pp. 3525–3533, Dec. 2009.
- [22] E. J. Naglich *et al.*, "Extended passband bandstop filter cascade with continuous 0.856-6-GHz coverage," *IEEE Trans. Microw. Theory Techn.*, vol. 60, no. 1, pp. 21–30, Jan. 2012.
- [23] H. Joshi *et al.*, "Highly loaded evanescent cavities for widely tunable high-Q filters," in *IEEE MTT-S Int. Microw. Symp. Dig.*, Jun. 3–8, 2007, pp. 2133–2136.
- [24] Y. Zheng *et al.*, "Compact substrate integrated waveguide tunable filter based on ferroelectric ceramics," *IEEE Microw. Wireless Compon. Lett.*, vol. 21, no. 9, pp. 477–479, Sep. 2011.
- [25] V. Sekar *et al.*, "A 1.216-GHz substrate-integrated-waveguide RF MEMS tunable filter," *IEEE Trans. Microw. Theory Techn.*, vol. 59, no. 4, pp. 866–876, Apr. 2011.
- [26] S. Adhikari *et al.*, "Simultaneous electric and magnetic two-dimensionally tuned parameter-agile SIW devices," *IEEE Trans. Microw. Theory Techn.*, vol. 61, no. 1, pp. 423–435, Jan. 2013.
- [27] H. H. Sigmarsson *et al.*, "In-situ control of tunable evanescent-mode cavity filters using differential mode monitoring," in *IEEE MTT-S Int. Microw. Symp. Dig.*, Jun. 7–12, 2009, pp. 633–636.
- [28] L. D. Landau and E. M. Lifschitz, *Electrodynamics of Continuous Media*. Oxford, U.K.: Pergamon, 1987, p. 19.
- [29] H. B. Palmer, "The capacitance of a parallel-plate capacitor by the Schwartz–Christoffel transformation," *Trans. Amer. Inst. Elect. Eng.*, vol. 56, no. 3, pp. 363–366, Mar. 1937.
- [30] R. S. Kwok and J.-F. Liang, "Characterization of high-Q resonators for microwave filter applications," *IEEE Trans. Microw. Theory Techn.*, vol. 47, no. 1, pp. 111–114, Jan. 1999.
- [31] H. H. Sigmarsson *et al.*, "Substrate integration of widely tunable bandpass filters," in *Proc. Int. Microelectron. Packag. Soc. Microelectron. Symp.*, San Jose, CA, USA, 2009, pp. 711–716.
- [32] H. Joshi *et al.*, "High-Q narrowband tunable filters with controllable bandwidth," in *IEEE MTT-S Int. Microw. Symp. Dig.*, Jun. 2009, pp. 629–632.
- [33] J. S. Hong and M. J. Lancaster, *Microstrip Filters for RF/Microwave Applications*. New York, NY, USA: Wiley, 2001.
- [34] S. Amari and F. Seyfert, "Design of dual-mode ridge cavity filters," in *IEEE MTT-S Int. Microw. Symp. Dig.*, Jun. 7–12, 2009, pp. 1625–1628.
- [35] X. Liu *et al.*, "Power handling of electrostatic MEMS evanescent-mode (EVA) tunable bandpass filters," *IEEE Trans. Microw. Theory Techn.*, vol. 60, no. 2, pp. 270–283, Feb. 2012.



**Eric J. Naglich** (S'09) received the B.S.E.C.E. degree from Purdue University, West Lafayette, IN, USA, in 2007, and is currently working toward the Ph.D. degree in electrical and computer engineering at Purdue University.

From 2007 to 2009, he was with the Edison Engineering Development Program of GE Healthcare. His current research focuses on tunable filter synthesis and fabrication for widely tunable adaptive RF front ends.



**Juseop Lee** (A'02–M'03) received the B.E. and M.E. degrees in radio science and engineering from Korea University, Seoul, Korea, in 1997 and 1999, respectively, and the Ph.D. degree in electrical engineering from The University of Michigan at Ann Arbor, Ann Arbor, MI, USA, in 2009.

In 1999, he joined LG Information and Communications (now LG Electronics), Korea, where his activities included design and reliability analysis of RF components for code-division multiple-access (CDMA) cellular systems. In 2001, he joined the

Electronics and Telecommunications Research Institute (ETRI), Korea, where he was involved in designing passive microwave equipment for  $K_u$ - and  $K_a$ -band communications satellites. In 2005, he joined The University of Michigan at Ann Arbor, where he was a Research Assistant and Graduate Student Instructor with the Radiation Laboratory, and his research activities focused on millimeter-wave radars and synthesis techniques for multiple-passband microwave filters. In 2009, he joined Purdue University, West Lafayette, IN, USA, where he was a Post-Doctoral Research Associate, and his activities included the design of adaptable RF systems. In 2012, he joined the Department of Computer and Communications Engineering, Korea University, Seoul, Korea, where he is currently an Assistant Professor. His research interests include RF and microwave components, satellite transponders, and electromagnetic theories. He is listed in *Who's Who in America*.

Dr. Lee was a recipient of the Highest Honor Award presented by Korea University, the Undergraduate Fellowship presented by Korea University, the Graduate Fellowship presented by LG Information and Communications, and the Graduate Fellowship presented by the Korea Science and Engineering Foundation. He was a recipient of the Rackham Predoctoral Fellowship presented by Rackham Graduate School, The University of Michigan at Ann Arbor. He was also the recipient of the IEEE Microwave Theory and Techniques Society (IEEE MTT-S) Graduate Fellowship. He was also the recipient of the 2nd Place Award of the 2010 IEEE MTT-S International Microwave Symposium Student Paper Competition.



**Hjalti H. Sigmarsson** (S'01–M'10) received the B.S.E.C.E. degree from the University of Iceland, Reykjavik, Iceland, in 2003, and the M.S.E.C.E. and Ph.D. degrees in electrical and computer engineering from Purdue University, West Lafayette, IN, USA, in 2005 and 2010, respectively.

He is currently an Assistant Professor with the School of Electrical and Computer Engineering, University of Oklahoma, Norman, OK, USA, where he teaches electromagnetic field theory, circuit theory, and filter design and synthesis. He is a member of the Advanced Radar Research Center (ARRC). His current research focuses

on reconfigurable RF and microwave hardware for agile communications, measurement, and radar systems. Furthermore, his research interests include spectral management schemes for cognitive radio architectures and advanced packaging utilizing heterogeneous integration techniques.

Dr. Sigmarsson is a member of the IEEE Microwave Theory and Techniques Society (IEEE MTT-S) and the International Microelectronics and Packaging Society (IMAPS). He was the recipient of the Best Paper Award of the IMAPS 2008 41st International Symposium on Microelectronics.



**Dimitrios Peroulis** (S'99–M'04) received the Ph.D. degree in electrical engineering from The University of Michigan at Ann Arbor, Ann Arbor, MI, USA, in 2003.

Since August 2003, he has been with Purdue University, where he currently leads a group of graduate students on a variety of research projects in the areas of RF microelectromechanical systems (MEMS), sensing, and power-harvesting applications, as well as RF identification (RFID) sensors for the health monitoring of sensitive equipment. He has been

Principal Investigator (PI) or a co-PI of numerous projects funded by government agencies and industry in these areas. He has been a key contributor on developing very high quality factor ( $Q > 1000$ ) RF MEMS tunable filters in mobile form factors. Furthermore, he has been involved in the investigation of failure modes of RF MEMS and MEMS sensors through the Defense Advanced Research Projects Agency (DARPA) MEMS/nanoelectromechanical systems (NEMS) Science and Technology Fundamentals Program (Phases I and II) and the Center for the Prediction of Reliability, Integrity and Survivability of Microsystems (PRISM) funded by the National Nuclear Security Administration.

Dr. Peroulis was the recipient of the National Science Foundation CAREER Award in 2008. His students have been the recipients of numerous Student Paper Awards and other student research-based scholarships. He is a Purdue Univer-

sity Faculty Scholar and has been the recipient of ten teaching awards, including the 2010 HKN C. Holmes MacDonald Outstanding Teaching Award and the 2010 Charles B. Murphy Award, which is Purdue University's highest undergraduate teaching honor.



**William J. Chappell** (S'98–M'02–SM'10) received the B.S.E.E., M.S.E.E., and Ph.D. degrees from The University of Michigan at Ann Arbor, Ann Arbor, MI, USA, in 1998, 2000, and 2002, respectively.

He is currently a Professor with the School of Electrical and Computer Engineering, Purdue University, West Lafayette, IN, USA, where he is also a member of the Birck Nanotechnology Center and the Center for Wireless Systems and Applications. His research focus is on advanced applications of RF and microwave components. He has

been involved with numerous Defense Advanced Research Projects Agency (DARPA) projects involved in advanced packaging and material processing for microwave applications. His research sponsors include the Homeland Security Advanced Research Projects Agency (HSARPA), the Office of Naval Research (ONR), the National Science Foundation (NSF), the State of Indiana, the Communications-Electronics Research, Development, and Engineering Center (CERDEC), and the Army Research Office (ARO), as well as industry sponsors. His research group uses electromagnetic analysis, unique processing of materials, and advanced design to create novel microwave components. His specific research interests are the application of very high quality factor and tunable components utilizing multilayer packages. In addition, he is involved with high-power RF systems, packages, and applications.

Dr. Chappell was the IEEE Microwave Theory and Techniques Society (IEEE MTT-S) Administrative Committee (AdCom) secretary for 2009 and was elected to the IEEE MTT-S AdCom for 2010–2012.